Available online at www.sciencedirect.com
SCIENCE DIRECT
International Journal of Heat and Mass Transfer 49 (2006) 377–386
International Journal of HEAT and MASS TRANSFER
www.elsevier.com/locate/ijhmt

Two-fluid modeling for low-pressure subcooled flow boiling

J.L. Xu [a], T.N. Wong [b,*], X.Y. Huang [b]

[a] Guangzhou Institute of Energy Conversion, Chinese Academy of Sciences, No. 81 Xianlie Zhong Rd., Guangzhou 510070, PR China
[b] School of Mechanical and Production Engineering, Nanyang Technological University, Nanyang Avenue, Singapore 639798, Singapore

Received 9 November 2003; received in revised form 30 September 2004
Available online 30 September 2005

Abstract

In the advanced electronic packaging, low-pressure subcooled flow boiling has been applied in design of compact heat exchangers for the effective electronic cooling. Through literature survey it is noted that little studies were carried out on the low-pressure and low-flow velocity subcooled flow boiling. In this paper a one-dimensional, non-equilibrium two-fluid model is proposed. The model has been validated with existing data in literature for both vertical up-flow and down-flow configurations. The simulated results show that under low-flow velocity the single phase heat transfer fraction is insignificant in vapor generation rate. The predicted results indicate that buoyancy force plays an important role on the void fraction evolvement, especially under low-flow velocity in vertical down-flow configuration.

Keywords: Subcooled flow boiling; Void fraction; Two-fluid; Vapor generation

1. Introduction

Subcooled boiling occurs when there is local boiling at the wall surface heated by the high heat fluxes, even though the bulk liquid has not reached the saturated temperature. The bubbles formed at the heated surface have a larger population density and short lifetime. Although the subcooled flow boiling improves the heat transfer, the pressure drop is increased such that the flow reduction and flow instability may occur. Fig. 1 shows the typical axial distribution of the temperature, void fraction, and bubble layer development along a uniformly heated channel, as illustrated by Srizawa and Kenning [1]. In the region of single-phase heat transfer, the temperature of the bulk liquid and the wall increases linearly along the tube. If the heating surface temperature exceeds the saturated temperature by a certain value, bubbles begin to initiate at a point called the onset of nucleation boiling (ONB, point A in Fig. 1), and they adhere and slide along the wall surface. The subcooled boiling continues downstream from ONB, due to the continuous wall heating. The bubble density increases and the bubble layer grows until the first bubble detaches from the heated surface into the core flow at point C. This low void fraction region continues until the void fraction starts to increase sharply at point D, the onset of significant void point (OSV). Finally the bulk liquid reaches to the saturated temperature.

In the advanced electronic packaging, low-pressure subcooled flow-boiling has been applied in the design of compact heat exchangers for the effective electronic

* Corresponding author.

0017-9310/$ - see front matter © 2005 Elsevier Ltd. All rights reserved.
doi:10.1016/j.ijheatmasstransfer.2004.12.051

Nomenclature

a	thermal diffusivity, m^2/s
a_G	sound speed of vapor, m/s
A	tube or annuli flow cross-section area, m^2
B	defined in Eq. (20)
C	defined in Eq. (21)
C_1	the portion of the heating surface not covered by bubbles
C_2	coefficient related to the pumping factor, $C_2 = \frac{1}{1+\varepsilon}$
C'	virtual mass coefficient
C_D	drag coefficient for a single bubble
C_{EV}	evaporation parameter with a value of about 0.5
C_{FI}	interfacial friction factor
C_{con}	empirical coefficient in Eqs. (41) and (42)
C_P	specific heat, J/kg °C
d_{BA}	bubble departure diameter, m
D	tube inside diameter, m
D_h	hydraulic diameter, $D_h = D$ for the tube channel, $D_h = D_o - D_i$ for the annular channel, m
D_i	the outside diameter of the inner tube for the annular channel, m
D_o	the inside diameter of the out tube for the annular channel, m
f_{GO}	single phase friction coefficient for vapor
f_{LO}	single phase friction coefficient for liquid
F_{GI}	interfacial force for the vapor due to the mass exchange, N/m^3
F_{LG}	interfacial force between the two phases, N/m^3
F_{LI}	interfacial force for the liquid due to the mass exchange, N/m^3
F_{WG}	force between the wall surface and the vapor, N/m^3
F_{WL}	force between the wall surface and the liquid, N/m^3
g	gravity acceleration, m/s^2
G	mass flux flowing in the tube, kg/m^2s
h	enthalpy, J/kg
h_{LG}	evaporation heat from the liquid to the vapor, J/kg
$\tilde{h}_{sp}$	single phase heat transfer coefficient, W/m^2 K
Ja	Jacob number in terms of the liquid subcooling, $\frac{\rho_L C_{PL}(T_{sat}-T_L)}{\rho_G h_{LG}}$
K	thermal conductivity, W/m K
L	length, m
L_{sp}	length of single phase flow, given in Eq. (59)
N	total node points divided for the channel
Nu_1	Nusselt number defined in Hainoun et al. [13]
Nu_2	Nusselt number defined in Hainoun et al. [13]
Nu_{sp}	Nusselt number for single phase flow
P	pressure, Pa
P_h	heating perimeter of the channel, m
Pr	Prandtl number
q_L	heat flux component for the heating of the liquid, W/m^2
q_P	heat flux component due to the pumping effect, W/m^2
q_V	heat flux component for generation the vapor on the wall surface, W/m^2
q_W	total wall heat flux, W/m^2
R_B	bubble radius, m
Re_B	bubble Reynolds number
Re_{GO}	vapor Reynolds number assuming that the whole mixture is flowing as vapor
Re_{LO}	liquid Reynolds number assuming that the whole mixture is flowing as liquid
t	time, s
T	temperature, °C
$T_{W,ONB}$	wall temperature at the onset of nucleation boiling, °C
U	velocity, m/s
U_{GJ}	bubble relative velocity, m/s
x	vapor mass quality
x_{eq}	equilibrium thermodynamic quality
Y	defined in Eq. (19)
z	axial location along the flow direction, m

Greek symbols

α	void fraction
α_{OSV}	void fraction at the onset of significant void
α_K	void fraction for phase K
ε	pumping factor
ε_1	initial assumed void fraction at ONB
ε_2	initial assumed relative velocity at ONB
μ	dynamic viscosity, Pa s
ρ	density, kg/m^3
τ_C	condensation time, s
σ	surface tension, N/m
Γ	vapor or liquid generation rate per unit mixture volume, kg/m^3 s
$\Gamma_{G,con}$	vapor condensation rate in the bulk core, kg/m^3 s
$\Gamma_{G,V}$	vapor production rate by the wall heating, kg/m^3 s
$\Gamma_{G,net}$	net vapor generation rate in terms of the balance of the wall heating and the condensation in the bulk core, kg/m^3 s
η	phase distribution parameter, $\eta = 0.5$ for bubbly flow, and $\eta = 0$ for other flow regime
θ	angle versus the gravity direction

δ_{th}	thermal boundary layer thickness, m
$\Delta\rho$	$\rho_L - \rho_G$
ΔP_{GO}	friction pressure drop assuming all the mixture is flowing as vapor
ΔP_{LO}	friction pressure drop assuming all the mixture is flowing as liquid
Δz	mesh size, m

Subscripts

0	the first node point in the two-phase flow region
B	bubbles
con	condensation
in	parameters at the location of the channel entrance
L	liquid
LG	values between vapor and liquid
G	vapor
ONB	point of onset of nucleation boiling
OSV	point of onset of significant void
sat	saturated
W	wall

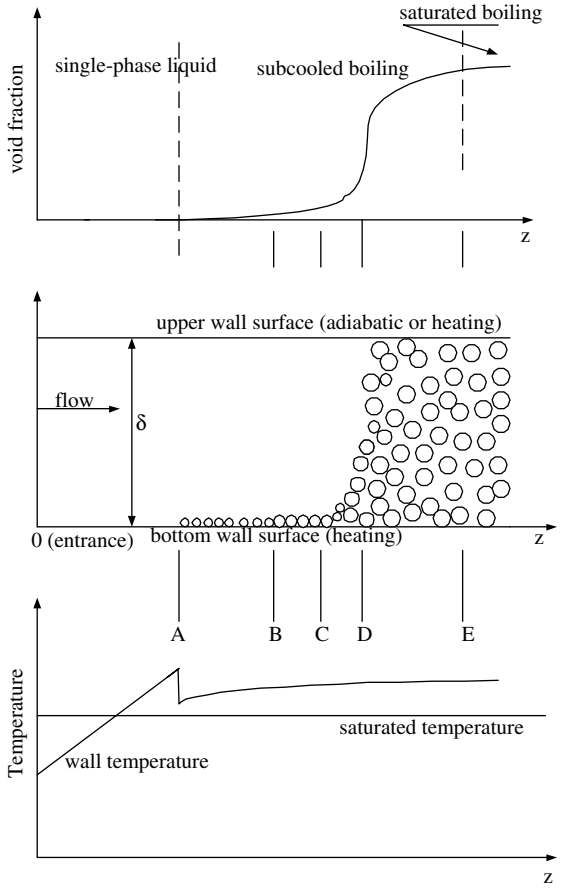

Fig. 1. Void fraction and temperature development in a heated channel.

cooling [2], due to its ability to enhance higher heat dissipated rate from the device. Literature review [3] shows that the existing theoretical models on subcooled flow boiling focused mainly on the study of void growth distribution at pressurized water reactor at high pressures. The application of the existing models to the subcooled flow boiling at low pressures was found to be unsatisfactory, as reported by Hainoun et al. [3], and Zeitoun et al. [4].

In experimental investigation, Rogers et al. [5] performed the low-pressure subcooled boiling experiments to determine the void content at OSV. The results have shown that the void fraction at OSV was in the range of 5–10%. Bibeau et al. [6] measured the void fraction and wall temperatures for two annular channels at low pressures. They found that the void growth in this high subcooled region was significant, which was quite distinct from the characteristics at high-pressures. The author reported that for low-pressure subcooled flow boiling, the OSV was independent of the location of the first bubble detaching from the heating surface and the transition took place from the partial boiling to the fully developed boiling. So far most of the measurements were performed for vertical up-flow configuration. Little investigation was performed on void growth in vertical down-flow [7].

In mathematical modeling two approaches were proposed to calculate the void evolvement in the subcooled flow boiling, one was the profile-fit model, the other was the mechanistic model. It is noted that the profile-fit models do not attempt to model the mechanism of the subcooled boiling, in which the effect of buoyancy force and the detachment mechanism in the determination of void content are ignored. This model is usually based on a fit to uniform axial heat flux data. The prediction of the subcooled void distribution for non-uniform axial heat flux is questionable, as reported by Levy [8] and Staub [9].

Hainoun et al. [3] proposed a vapor generation model to simulate the subcooled flow boiling. The numerical predictions compared reasonable well with the experiment data. A mechanistic model was developed by Zeitoun et al. [4] to predict the axial void fraction profile in low-pressure subcooled flow boiling, in which the effect of buoyancy force was not considered. This buoyancy force effect will become significant at low-flow velocity in vertical down-flow configuration.

The present investigation is motivated by the need to model the low-pressure subcooled flow boiling in the cooling of electronic devices operating at low-flow velocity. A one-dimensional, non-equilibrium two-fluid model is developed. The two-phases are modeled using the separated equations accounting for the interfacial forces between the phases. The model accounts for the flow direction in both the vertical upward and downward configurations and flow pattern transitions.

2. Mathematical models

2.1. Governing equations

Referring to Fig. 1, the subcooled liquid enters the gap channel formed by two infinity plates with the gap of δ. The bottom wall is being heated, while the upper wall is adiabatic or heated. The flow is considered to be one-dimensional with accounting for the average parameter in the height direction while the width direction is infinity. Heating causes the onset of boiling taking place somewhere downstream of the entrance. In the two-phase region, formulation of the general conservation equations of mass, momentum and energy was presented by Ishii and Mishima [10]. For the steady state with negligible kinetic and potential energy, the conservation equations are reduced to the following five equations. It is noted that the following conservation equations are general and are valid for the low pressure and mass flux operation ranges.

- Phase mass equations

$$\frac{\partial}{\partial z}(\alpha\rho_G U_G) = \Gamma_G \tag{1}$$

$$\frac{\partial}{\partial z}[(1-\alpha)\rho_L U_L] = \Gamma_L \tag{2}$$

- Phase momentum equations

$$\frac{\partial}{\partial z}(\alpha\rho_G U_G^2) + \alpha\frac{\partial P}{\partial z} + \alpha\rho_G g\cos(\theta) = -F_{WG} - F_{LG} - F_{GI} \tag{3}$$

$$\frac{\partial}{\partial z}[(1-\alpha)\rho_L U_L^2] + (1-\alpha)\frac{\partial P}{\partial z} + (1-\alpha)\rho_L g\cos(\theta) = -F_{WL} + F_{LG} - F_{LI} \tag{4}$$

- Mixture energy equation

$$\frac{\partial}{\partial z}(\alpha\rho_G U_G h_G + [1-\alpha]\rho_L U_L h_L) = \frac{q_W P_h}{A} \tag{5}$$

It is assumed that the wall shear stress contributed by the vapor phase (F_{WG}) is negligible [11]. Note that $\Gamma_G + \Gamma_L = 0$. q_W is the applied wall heat flux, P_h is the heated perimeter and A is the flow cross-section area of the channel. P_h is πD_i for annular channels with the heating on the inner wall surface. The liquid density ρ_L is the functions of the pressure and enthalpy.

$$\rho_L = \rho_L(P, h_L) \tag{6}$$

The vapor phase is assumed to be saturated thus the vapor density and the enthalpy are only depended on the pressure.

$$\rho_G = \rho_{G,sat}(P) \tag{7}$$

$$h_G = h_{G,sat}(P) \tag{8}$$

Eqs. (1)–(5) contain five unknowns, α, P, U_G, U_L, h_L. The liquid temperature is known from the liquid enthalpy h_L and pressure P.

2.2. The determination of the interfacial terms

2.2.1. Interfacial drag force between the two-phases

Interfacial drag force between the two phases F_{LG} is modeled as [11]

$$F_{LG} = \frac{2C_{FI}}{D_h}\sqrt{\alpha}\rho_G(U_G - U_L)\mid U_G - U_L \mid + C'\alpha\rho_L U_G\frac{d(U_G - U_L)}{dz} \tag{9}$$

where C' is a virtual mass coefficient, taken as $C' = 0.5$ for bubbly flow and $C' = 0$ for other flow regimes. The interfacial friction factor C_{FI} is taken as

$$C_{FI} = \begin{cases} C_D\sqrt{\alpha}(1-\alpha)^{-1.7}\dfrac{\rho_L}{\rho_G}\dfrac{D_h}{2R_B} \\ \text{bubbly flow } (\alpha \leqslant 0.25) \\ 0.005(1+75(1-\alpha)) \\ \text{annular flow } (\alpha \geqslant 0.8) \end{cases} \tag{10}$$

In the churn turbulent flow with medium void fraction between the bubbly and annular flow, C_{FI} is interpolated linearly with void fraction between the two values given in Eq. (10). The drag coefficient for a single bubble C_D, in Eq. (10), depends on the bubble Reynolds number Re_B

$$C_D = \begin{cases} \dfrac{24}{Re_B}(1 + 0.15Re_B^{0.687}) & Re_B < 1000 \\ 0.44 & Re_B \geqslant 1000 \end{cases} \tag{11}$$

where the bubble Reynolds number Re_B is defined as

$$Re_B = \frac{2\rho_L R_B(1-\alpha)\mid U_G - U_L \mid}{\mu_L} \tag{12}$$

Note that F_{LG} in Eq. (9) is positive for vertical upward flow ($U_G > U_L$), and negative for vertical downward flow ($U_G < U_L$).

2.2.2. Shear stress between the liquid phase and the tube wall

The wall liquid friction F_{WL} is modeled by the Chisholm's correlation [12], since such correlation fits the advanced empirical correlation curves of Baroczy quite well and accounts for the effect of mass flux on the friction pressure gradient. The correlation is expressed by the following set of equations:

$$F_{WL} = \lfloor 1 + (Y^2 - 1)(Bx^{(2-n)/2}(1-x)^{(2-n)/2} + x^{2-n}) \rfloor \Delta P_{LO} \tag{13}$$

$$\Delta P_{LO} = \frac{4}{D_h} f_{LO} \frac{G^2}{2\rho_L} \tag{14}$$

where ΔP_{LO} is the single phase friction pressure drop which would exist if the total mass flow of two phase mixture flowed as liquid phase only, n is the power in the friction factor–Reynolds number relationship ($n = 0.25$ for the Blasius equation). Y is a property coefficient defined by the square root of the ratio between the pressure gradient due to friction if the total mixture flows as vapor only and that if the total mixture flows as liquid only, i.e.,

$$Y = \left(\frac{\Delta P_{GO}}{\Delta P_{LO}}\right)^{0.5} = \left(\frac{f_{GO}\rho_L}{f_{LO}\rho_G}\right)^{0.5} \tag{15}$$

The coefficient B in Eq. (13) is given by

$$B = \frac{CY - 2^{2-n} + 2}{Y^2 - 1} \tag{16}$$

where

$$C = \frac{U_L}{U_G}\sqrt{\frac{\rho_L}{\rho_G}}\left(1 + \frac{U_G^2}{U_L^2}\frac{\rho_G}{\rho_L}\right) \tag{17}$$

The true vapor mass quality x can be calculated as

$$x = \frac{1}{1 + \frac{1-\alpha}{\alpha}\frac{\rho_L}{\rho_G}\frac{U_L}{U_G}} \tag{18}$$

In Eq. (14) f_{LO} is the single-phase friction coefficient determined from

$$f_{LO} = \frac{16}{Re_{LO}} \text{ for } Re_{LO} = \frac{GD_h}{\mu_L} \leqslant 2000 \tag{19}$$

$$f_{LO} = 0.079 Re_{LO}^{-0.25} \text{ for } Re_{LO} = \frac{GD_h}{\mu_L} > 2000 \tag{20}$$

In Eq. (15) f_{GO} is determined from equations similar to Eqs. (19) and (20), but involving the vapor properties.

2.2.3. Determination of F_{GI} and F_{LI}

The momentum exchange between the phases, F_{GI} and F_{LI}, due to the mass exchange, are modeled as:

$$F_{GI} = \eta(U_G - U_L)\Gamma_G \tag{21}$$

$$F_{LI} = (1-\eta)(U_L - U_G)\Gamma_L \tag{22}$$

$\eta$is the phase distribution factor, $\eta = 0.5$ for bubbly flow, and $\eta = 0$ in other flow regime.

2.3. Vapor generation rate

After ONB, bubbles appearing on the heating surface may condense in the bulk flow as they recede from the surface. The net amount of vapor generation rate is determined by the difference between the vapor generation rate at the wall and the condensation rate in the bulk. A correlation by Bergels et al. [13] is used to determine the wall overheating at which the first nuclei is activated

$$T_W - T_{sat} = \frac{5}{9}\left(\frac{q_W}{1100}P^{-1.156}\right)^{0.463P^{0.0234}} \tag{23}$$

The left hand of the above equation is the wall superheating. P is the pressure in bar. q_W has the unit of W/m^2.

In the subcooled region, the wall heat flux can be divided into three components, i.e. the vapor generation term q_V, single phase forced convection fraction, and the "pumping effect", q_p due to the agitation of the thermal boundary layer caused by the bubble growth-collapse cycle. The last two terms are combined together to contribute the sensible heating of the bulk liquid.

$$q_W = q_V + C_1\tilde{h}_{sp}(T_W - T_L) + q_p \tag{24}$$

where C_1 accounts for the portion of the heating surface which is not cover by bubbles. C_1 is dependent on the void fraction. The heating surface is not directly accessible to liquid as the void content increases since more bubbles cover the heating surface. Hainoun et al. [3] suggested that C_1 can be expressed as:

$$\begin{aligned} C_1 &= 1 - \frac{\pi}{16}\frac{\alpha}{\alpha_{OSV}} \quad \text{for } \alpha \leqslant \frac{16\alpha_{OSV}}{\pi} \\ C_1 &= 0 \qquad\qquad\quad \text{for } \alpha > \frac{16\alpha_{OSV}}{\pi} \end{aligned} \tag{25}$$

where α_{OSV} is the void content at OSV.

$\tilde{h}_{sp}$ is the single-phase heat transfer coefficient and the wall temperature T_W is predicted by Shah [14].

Define pumping factor as the ratio between the pumping component and the vapor component, $\varepsilon = \frac{q_p}{q_V}$. Thus q_V is given as:

$$q_V = \frac{q_W - C_1\tilde{h}_{sp}(T_W - T_L)}{1 + \varepsilon} \tag{26}$$

Introduce another coefficient C_2 to relate the pump factor as

$$C_2 = \frac{1}{1 + \varepsilon} \tag{27}$$

Eq. (26) is rewritten as

$$q_V = C_2(q_W - C_1\tilde{h}_{sp}[T_W - T_L]) \tag{28}$$

The pumping factor can be calculated from Zeitoun and Shoukri [4] as

$$\varepsilon = \frac{3}{4}\frac{\rho_L C_{PL}(T_W - T_L)}{\rho_G h_{LG}}\frac{\delta_{th}}{2R_B} \tag{29}$$

where the thermal boundary layer thickness δ_{th} is defined as

$$\delta_{th} = \frac{k_L(T_W - T_L)}{q_W} \tag{30}$$

Alternatively, Yang and Weisman [15] correlated the pumping factor based on their experimental data as

$$\varepsilon = 3\frac{h_{L,sat} - h_L}{h_{LG}} \tag{31}$$

Note that, Eq. (31) is only valid for R113, which needs more verification before it is extended to other working fluids.

The coefficient C_2 can be determined once ε is established. Alternatively, the C_2 expression developed by Hainoun et al. [3] can be used

$$C_2 = 2C_{EV}\left(\frac{T_W - T_{sat}}{T_W - T_L}\right)^2 \tag{32}$$

where C_{EV} is an evaporation parameter with a value of about 0.5.

Hence the vapor production rate on the wall surface is given as

$$\Gamma_{G,V} = \frac{q_V P_h}{A h_{LG}} \tag{33}$$

2.3.1. Bubble condensation rate

Hainoun et al. [3] assumed that bubble condensation is dependent on the Jacob number. Heat transfer at the phase boundary largely determines condensation when the Jacob number is less than 80. Inertia effects are dominant if the Jacob number is larger than 100. In transition region ($80 < Ja < 100$) both the heat transfer and the inertia effects are of significance. The inertia-controlled condensation is written as

$$\Gamma_{G,con} = C_{con}\rho_G\frac{\alpha}{\tau_C} \tag{34}$$

where τ_C is the condensation time after Rayleigh.

In the heat transfer dominant region, the condensation rate is modeled in terms of the bulk Reynolds number as

$$\Gamma_{G,con} = C_{con}3.6\frac{\alpha}{d_{BA}^2}\rho_G a Nu_1 Ja \quad \text{for } Re < 10^4 \tag{35}$$

$$\Gamma_{G,con} = C_{con}3.6\frac{\alpha}{d_{BA}D_h}\rho_G a Nu_2 Ja \quad \text{for } Re > 3\times 10^4 \tag{36}$$

C_{con} has the empirical value of 0.16 through comparing with the experimental data. The determination of τ_C, d_{BA}, Nu_1 and Nu_2 can be found in Hainoun et al. [3].

Hence the net vapor generation rate is determined by the difference between the vapour generation rate at the wall and the condensation rate in the bulk

$$\Gamma_{G,net} = \frac{q_V P_h}{A h_{LG}} - \Gamma_{G,con} \tag{37}$$

3. Solution procedure

With the assumption that the vapor phase is saturated, thus the vapor density and enthalpy are dependent on pressure, the differential terms $\frac{\partial\rho_G}{\partial z}$, and $\frac{\partial h_G}{\partial z}$ can be replaced by the differential terms of $\frac{\partial P}{\partial z}$ by

$$\frac{\partial\rho_G}{\partial z} = \frac{\partial\rho_G}{\partial P}\frac{\partial P}{\partial z} = \frac{1}{a_G^2}\frac{\partial P}{\partial z} \tag{38}$$

$$\frac{\partial h_G}{\partial z} = \frac{\partial h_G}{\partial P}\frac{\partial P}{\partial z} \tag{39}$$

The liquid density is dependent on pressure and enthalpy. Thus $\frac{\partial\rho_L}{\partial z}$ can be replaced by:

$$\frac{\partial\rho_L}{\partial z} = \left.\frac{\partial\rho_L}{\partial h_L}\right|_P\frac{\partial h_L}{\partial z} + \left.\frac{\partial\rho_L}{\partial P}\right|_{h_L}\frac{\partial P}{\partial z} \tag{40}$$

Substituting Eqs. (38)–(40) into the partial differential Eqs. (1)–(5), we obtained:

$$\rho_G U_G\frac{\partial\alpha}{\partial z} + \frac{\alpha U_G}{a_G^2}\frac{\partial P}{\partial z} + \alpha\rho_G\frac{\partial U_G}{\partial z} = \Gamma_G \tag{41}$$

$$-\rho_L U_L\frac{\partial\alpha}{\partial z} + (1-\alpha)U_L\left.\frac{\partial\rho_L}{\partial P}\right|_{h_L}\frac{\partial P}{\partial z} + (1-\alpha)\rho_L\frac{\partial U_L}{\partial z} + (1-\alpha)U_L\left.\frac{\partial\rho_L}{\partial h_L}\right|_P\frac{\partial h_L}{\partial z} = \Gamma_L \tag{42}$$

$$\alpha\rho_G U_G\frac{\partial U_G}{\partial z} + \alpha\frac{\partial P}{\partial z} + \alpha\rho_G g\cos(\theta) = -F_{LG} - F_{GI} \tag{43}$$

$$(1-\alpha)\rho_L U_L\frac{\partial U_L}{\partial z} + (1-\alpha)\frac{\partial P}{\partial z} + (1-\alpha)\rho_L g\cos(\theta) = -F_{WL} + F_{LG} - F_{LI} \tag{44}$$

$$\alpha\rho_G U_G\frac{\partial h_G}{\partial P}\frac{\partial P}{\partial z} + (1-\alpha)\rho_L U_L\frac{\partial h_L}{\partial z} = \frac{q_W P_h}{A} - \Gamma_G(h_G - h_L) \tag{45}$$

Eqs. (41)–(45) can be expressed as Eq. (46) by choosing α, P, U_G, U_L, h_L as the dependent variables

$$\begin{bmatrix} \rho_G U_G & \dfrac{\alpha U_G}{a_G^2} & \alpha\rho_G & 0 & 0 \\ -\rho_L U_L & (1-\alpha)U_L \left.\dfrac{\partial\rho_L}{\partial P}\right|_{h_L} & 0 & (1-\alpha)\rho_L & (1-\alpha)U_L \left.\dfrac{\partial\rho_L}{\partial h_L}\right|_P \\ 0 & \alpha & \alpha\rho_G U_G & 0 & 0 \\ 0 & (1-\alpha) & 0 & (1-\alpha)\rho_L U_L & 0 \\ 0 & \alpha\rho_G U_G \dfrac{\partial h_G}{\partial P} & 0 & 0 & (1-\alpha)\rho_L U_L \end{bmatrix}_{i-1} \begin{bmatrix} \dfrac{\partial\alpha}{\partial z} \\ \dfrac{\partial P}{\partial z} \\ \dfrac{\partial U_G}{\partial z} \\ \dfrac{\partial U_L}{\partial z} \\ \dfrac{\partial h_L}{\partial z} \end{bmatrix}_i = \begin{bmatrix} B_1 \\ B_2 \\ B_3 \\ B_4 \\ B_5 \end{bmatrix}_{i-1} \tag{46}$$

Here

$$\left.\begin{aligned} B_1 &= \Gamma_{G,net} \\ B_2 &= -\Gamma_{G,net} \\ B_3 &= -F_{LG} - F_{GI} - \alpha\rho_G g\cos(\theta) \\ B_4 &= -F_{WL} + F_{LG} - F_{LI} - (1-\alpha)\rho_L g\cos(\theta) \\ B_5 &= \frac{q_W P_h}{A} - \Gamma_{G,net}(h_{G,sat} - h_L) \end{aligned}\right\} \tag{47}$$

Eq. (46) was solved using Runge–Kutta or Euler method for small mesh size.

3.1. Boundary condition

To start the computation, an initial void fraction (ε_1) and bubble relative velocity (ε_2) are used. The calculation shows that the range of ε_1=10^{-3}–10^{-5} and $\varepsilon_2 = 10^{-2}$–10^{-4} has no influence on the calculated void fraction. Note that ε_2 is positive for vertical up-flow, and negative for the vertical down-flow.

The boundary conditions of the two-phase at $z = z_{L_{sp}}$ are

$$\left.\begin{aligned} \alpha_0 &= \varepsilon_1 \\ P_0 &= P_{in} - \tfrac{4L_{sp}}{D_h} f_{LO} \tfrac{G^2}{2\rho_{L,in}} (P_{in} \text{ specified}) \\ U_{G,0} &= U_{L,0} + \varepsilon_2 \\ U_{L,0} &= \tfrac{G}{\rho_{L,ONB}} (G \text{ specified}) \\ h_{L,0} &= h_{L,ONB} \end{aligned}\right\} \tag{48}$$

Integration was performed from the ONB to the channel exit using the Gauss–Seidel iteration technique to solve the linear Eq. (46). Initially larger mesh sizes, corresponding to a small number of node points N are used. Then N is increased gradually to check its effect on the exit void fraction. Such process stopped until a very stable exit void fraction is reached. For most of our calculations, $N = 50$–100 has enough accuracy.

4. Results and discussion

4.1. Sensitivity analysis of coefficients C_1 and C_2

To validate the proposed model, comparisons have been made with the available experimental data published by Zeitoun and Shoukri [4]. Sensitivity analyses of coefficients C_1 and C_2 in the vapor generation equation were conducted. Curve 1 in Fig. 2 is plotted using $C_1 = 1.0$. Since α_{OSV} is in the range of 0.05–0.1 as reported by Rogers et al. [5], curves 2 and 3 are produced using Eq. (25) with α_{OSV} of 0.05 and 0.1, respectively. It is seen from Fig. 2 that the calculated void fractions are insensitive to the C_1 coefficient. The differences among the three curves can only be identified near the channel exit. The results indicated that under low-fluid velocity the single phase heat transfer fraction is insignificant in vapour generation. The void fraction is insensitive to the fraction of the heating surface covered by the fluid.

Fig. 3 shows the influence of C_2 on the void fraction. The result indicated that the pumping factor ε developed by Yang and Weisman [15] (curve 3) over-predicts the void fraction. Since the correlation was developed from the experimental data of R113, it is not suitable for water-steam system. The pumping factor developed by Zeitoun and Shoukri [4] (curve 1) also over-predicts the void fraction. Note that the C_2 coefficient by Hainoun et al. [3] (curve 2 using Eq. (32)) matches the experimental data very well. Based on the above analysis, the following coefficients were used in the subsequent void fraction modeling.

$$C_1 = 1$$

$$C_2 = 2C_{EV}\left(\frac{T_W - T_{sat}}{T_W - T_L}\right)^2$$

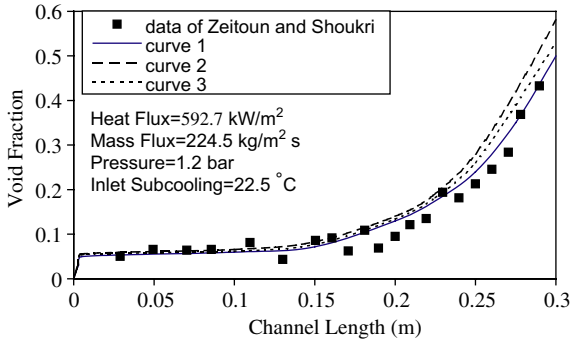

Fig. 2. Effect of C_1 coefficient on the void fraction.

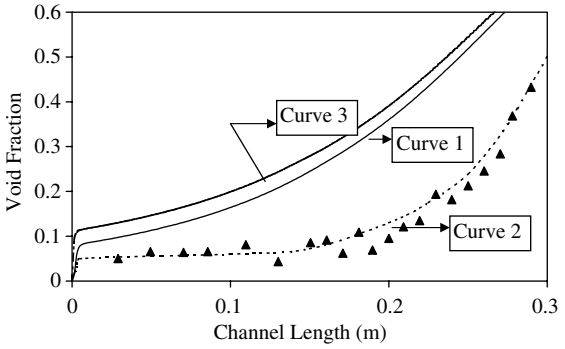

Fig. 3. Effect of C_2 coefficient on the void fraction.

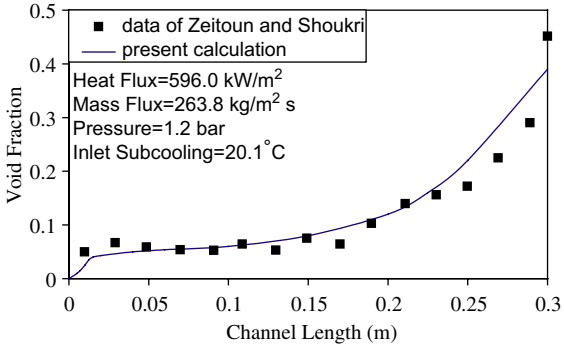

Fig. 4. Comparisons of model prediction with experimental data by Zeitoun and Shoukri [4].

4.2. Comparisons with the experimental data

To validate the proposed model, comparisons have been made with available experimental data by Donevski and Shoukri [16], Rogers et al. [5], and Zeitoun and Shoukri [4], Bibeau and Salcudean [7]. Their experimental set-up and flow conditions are summarized in Table 1. The experimental parameters cover the follow ranges: pressure of 1–2 bar, mass flux of 70–500 kg/m^2, and wall heat flux of 300–1000 kW/m^2.

Figs. 4 and 5 show that the proposed theoretical void fraction distributions agree well with the experiment data presented by Zeitoun et al. [4] and Rogers et al. [5] in vertical up-flow configuration.

Fig. 6 shows a comparison of the void fraction distribution along the tube with experimental results reported by Donevski et al. [16]. In the reported experiment, an adiabatic section was maintained after 0.4 m measured from the inlet. Again good agreement was obtained.

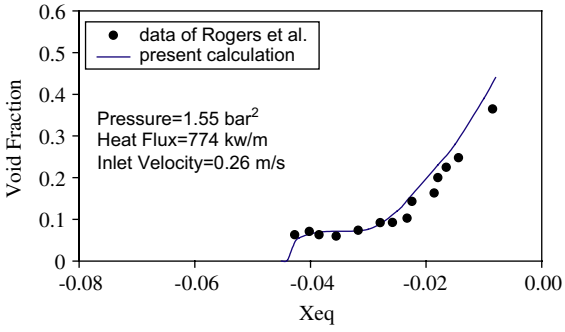

Fig. 5. Comparisons of the model prediction with experimental data by Rogers et al. [5].

4.3. Comparison between the vertical up-flow and down-flow

Fig. 7 shows the comparisons of void fractions for vertical up-flow and vertical down-flow. The good agreement between predicted value and experimental data presented by Bibeau et al. [7] indicates that the present model is applicable to both vertical up-flow and down-flow situation. The results show that for the same flow condition, higher void fraction prevails for vertical down-flow than that for vertical up-flow. The numerical results also show that OSV occurs early for vertical down-flow than that of up-flow. This is due to the reason that for vertical down-flow, the buoyancy force is opposite to the bulk flow hence a lower vapor velocity

Table 1
Various experimental set-up and flow condition for void fraction measurement

Authors	Annular gap dimension (mm)	Channel length (mm)	Flow direction	Pressure (bar)	Mass flux (kg/m^{2}s)	Heat flux (kw/m^2)	Inlet subcooling (°C)
Donevski and Shoukri [16]	25.0 mm OD, 12.7 mm ID	420	Vertical up-flow	1.687–1.735	420–430	576–594	30
Rogers et al. [5]	30.9 mm OD, 13.1 mm ID	480, 600	Vertical up-flow	1.50–1.55	70–450	300–1200	18–51
Zeitoun and Shoukri [4]	25.4 mm OD, 12.7 mm ID	300	Vertical up-flow	1.17–1.68	252.8–403.0	487.9–603.2	16.6–20.1
Bibeau and Salcudean [7]	21.8 mm OD, 12.7 mm ID	480	Vertical down-flow	1.55	220–450	300–900	10–85

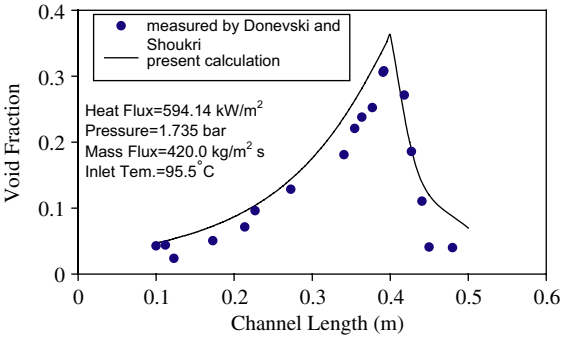

Fig. 6. Comparisons of model prediction with experimental data by Donevski and Shoukri [16].

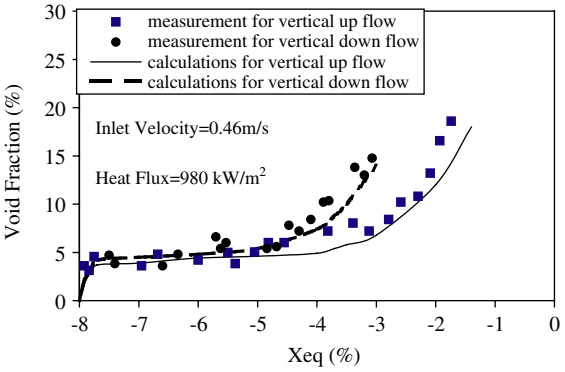

Fig. 7. Comparisons of model prediction with experimental data for both verticals up and down flow by Bibeau and Salcudean [7].

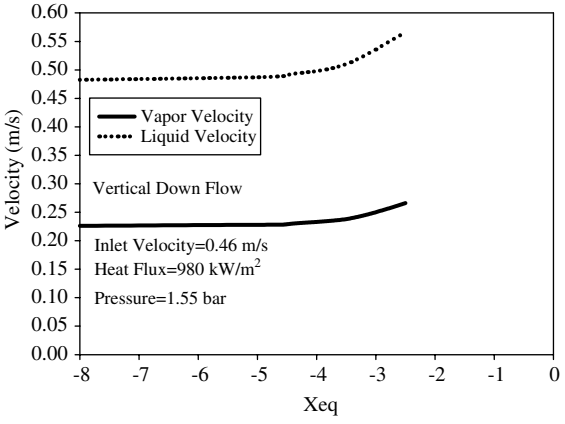

Fig. 8. Two phase velocity distribution against the thermodynamic quality.

is predicted. Fig. 8 shows the variation of liquid phase and vapor phase velocities against the quality. As the buoyancy force is opposite to the flow, vapor is difficult to move into the downward bulk flow hence vapor residing in the channel and a larger void fraction is resulted.

5. Conclusions

A one-dimensional, non-equilibrium two-fluid model has been developed for the predictions of low-pressure subcooled flow boiling. The model has been validated by the available experimental data for both vertical up-flow and down-flow.

The simulated results show that at low pressure the void fraction is insensitive to the fraction of the heating surface covered by the fluid. The predicted results highlight that buoyancy force plays an important role on the void fraction evolvement, especially at low velocity for vertical down-flow.

References

[1] A. Srizawa, D.B.R. Kenning, A Study of Forced Convective Subcooled Flow Boiling. Technical Report, Institute of Atomic Energy, Kyoto University, 1979.
[2] M. Bowers, Mudawar, High flux boiling in low flow rate, low pressure drop mini-channel and micro-channel heat sinks, Int. J. Heat Mass Transfer 37 (2) (1994) 321–332.
[3] A. Hainoun, E. Hicken, J. Wolters, Modeling of void formation in the subcooled boiling regime in the ATHLET code to simulate flow instability for research reactors, Nucl. Eng. Design 167 (1996) 175–191.
[4] O. Zeitoun, M. Shoukri, Axial void fraction profile in low pressure subcooled flow boiling, Int. J. Heat Mass Transfer 4 (4) (1997) 869–879.
[5] J.T. Rogers, M. Salcudean, Z. Abdullah, D. Mcledod, D. Poirier, The onset of significant void in up-flow boiling of water at low pressure and velocities, Int. J. Heat Mass Transfer 30 (11) (1987) 2247–2260.
[6] E.L. Bibeau, M. Salcudean, Subcooled void growth mechanisms and prediction at low pressure and low velocity, Int. J. Multiphase Flow 20 (5) (1994) 837–863.
[7] E.L. Bibeau, M. Salcudean, The effect of flow direction on void growth at low velocities and low pressures, Int. Commun. Heat Mass Transfer 17 (1990) 19–25.
[8] S. Levy, Forced convection subcooled boiling: prediction of vapour volumetric fraction, Int. J. Heat Mass Transfer 10 (1967) 951–965.
[9] F.W. Staub, The void fraction in subcooled boiling: prediction of the initial point of net vapor generation, J. Heat Transfer 90 (1968) 151–157.
[10] M. Ishii, K. Mishima, Two-fluid model and hydrodynamic constitutive relations, Nucl. Eng. Design 82 (1984) 107–126.
[11] H.J. Richter, Separated two-phase flow model: application to critical two phase flow, Int. J. Multiphase Flow 9 (5) (1983) 511–530.
[12] D. Chisholm, Pressure gradient due to friction during the flow of evaporating two phase mixtures in smooth

tubes and channel, Int. J. Heat Mass transfer 16 (1973) 347–358.
[13] A.E. Bergels, J.G. Collier, J.M. Delhaye, G.F. Hewitt, F. Mayinger, Two phase flow and heat transfer in the power and process industries, Hemisphere, Washington, DC, 1981.
[14] M.M. Shah, General prediction of heat transfer during subcooled flow boiling in annuli., Heat Transfer Eng. 4 (1983) 24–31.
[15] J.Y. Yang, J. Weisman, A phenomenological model of subcooled flow boiling in the detached bubble region, Int. J. Multiphase Flow 17 (1) (1991) 77–94.
[16] B. Donevski, M. Shoukri, Experimental study of subcooled flow boiling and condensation in an annular channel, Thermofluids Report no. ME/89/TF/R1, Department of Mechanical Engineering, McMaster University, Hamilton, ON, 1989.